

49
50

Chukochenite ($\text{Li}_{0.5}\text{Al}_{0.5}$) Al_2O_4 , a new lithium oxyspinel mineral from the Xianghualing skarn, Hunan Province, China

51
52

CAN RAO^{1*}, XIANGPING GU², RUCHENG WANG³, QUNKE XIA¹, YUANFENG CAI³, CHUANWAN
DONG¹, FRÉDÉRIC HATERT⁴, AND YANTAO HAO¹

53
54

¹ Key Laboratory of Geoscience Big Data and Deep Resource of Zhejiang Province, School of Earth
Sciences, Zhejiang University, Hangzhou 310027, China

55
56

² School of Earth Sciences and Info-physics, Central South University, Changsha, 410083, China

57
58

³ State Key Laboratory for Mineral Deposits Research, School of Earth Sciences and Engineering, Nanjing
University, Nanjing, 210046, China

59
60

⁴ Laboratoire de Minéralogie, B18, Université de Liège, B-4000 Liège, Belgium

61
62

*E-mail: canrao@zju.edu.cn

63
64

ABSTRACT

65
66

Chukochenite, ($\text{Li}_{0.5}\text{Al}_{0.5}$) Al_2O_4 , is a new mineral species from the Xianghualing skarn,
Hunan Province, southern China. It occurs as subhedral to euhedral crystals up to 200 μm
across in the green rock of Xianghualing skarn, closely associated with fluorite, phlogopite,
chrysoberyl, margarite, chlorite, ferronigerite-2N1S, and zinconigerite-2N1S. The crystals are
colorless and transparent with vitreous luster. Chukochenite is brittle with irregular fracture,
has a Mohs hardness of 8, and shows light red fluorescence under 253.7 nm UV radiation and
light green fluorescence under 365 nm UV radiation. The calculated density is 3.771 g/cm^3 .
Chukochenite is optically biaxial (-) with $\alpha = 1.79$ (2), $\beta = 1.82$ (2), and $\gamma = 1.83$ (2) (589 nm).
The calculated $2V$ is 60° , and optical orientation: X , Y and Z are parallel to crystallographic a ,
 b and c , respectively. Electron microprobe analysis (Li by LA-ICP-MS) yielded in wt.%
 Al_2O_3 80.70, Fe_2O_3 8.16, Li_2O 3.68, ZnO 3.25, MnO 2.49, MgO 1.70, Na_2O 0.11, CaO 0.08,
 TiO_2 0.02, K_2O 0.01, and Cr_2O_3 0.01 (total 100.24 wt.%), giving an empirical formula
 $[(\text{Li}_{0.355}\text{Al}_{0.138}\text{Na}_{0.005}\text{Ca}_{0.002})_{\Sigma 0.5}(\text{Al}_{0.145}\text{Fe}^{+3}_{0.147}\text{Mg}_{0.061}\text{Zn}_{0.058}\text{Mn}_{0.051}\text{Si}_{0.001})_{\Sigma 0.463}]\text{Al}_2\text{O}_4$ on the
basis of 4 O atoms per formula unit. Chukochenite is orthorhombic, *Imma*, $a = 5.659$ (1), $b =$

75
76
77
78

79 16.898 (1), $c = 7.994$ (1) Å, $V = 764.46$ (8) Å³, and $Z = 12$. The nine strongest lines of powder
80 XRD [d in Å (l) (hkl)] are: 2.405 (53) (231); 1.996 (29) (260); 1.535 (77) (303); 1.413 (100)
81 (264); 1.260 (52) (2 12 0); 1.068 (36) (1 13 4); 1.039 (61) (503); 0.999 (59) (008); and 0.942
82 (35) (3 13 4). Chukochenite has a framework structure of spinel with low symmetry
83 (orthorhombic *Imma*) due to the ordering of Li cations over octahedrally coordinated sites,
84 which has not been previously reported for synthetic $(\text{Li}_{0.5}\text{Al}_{0.5})\text{Al}_2\text{O}_4$. This structure type is
85 based on a framework of AlO_4 tetrahedra, AlO_6 and LiO_6 octahedra. AlO_6 edge-sharing
86 octahedra form chains along the a axis. AlO_6 octahedra and LiO_6 octahedra in a 2:1 ratio
87 share edges, forming octahedral chains along b . These octahedral chains are connected by
88 AlO_4 tetrahedra, and each corner of an AlO_4 tetrahedron shares with three AlO_6 octahedra or
89 two $\text{AlO}_6 +$ one LiO_6 octahedra. The discovery of chukochenite adds new perspective on the
90 cation ordering and the mechanism of luminescence and magnetism in $(\text{Li}_{0.5}\text{Al}_{0.5})\text{Al}_2\text{O}_4$.

91 **Key words:** Chukochenite, new mineral, $(\text{Li}_{0.5}\text{Al}_{0.5})\text{Al}_2\text{O}_4$, crystal structure, optical
92 property, XRD, EPMA, Raman spectroscopy

93

94

INTRODUCTION

95 The synthetic compound $(\text{Li}_{0.5}\text{Al}_{0.5})\text{Al}_2\text{O}_4$, when doped with trace metal ions such as Fe^{3+} ,
96 Eu^{3+} , Cr^{3+} , exhibits interesting magnetic and fluorescent properties, and thus the structures of
97 two forms differing in cation ordering have been extensively studied for potential materials
98 applications (*e.g.*, [Datta and Roy 1963](#); [Pott and Mcnicol 1973](#); [Singh and Rao 2008](#); [Xie et al. 2011](#)). Here, the corresponding natural phase, a new mineral chukochenite
99 $(\text{Li}_{0.5}\text{Al}_{0.5})\text{Al}_2\text{O}_4$, but with a different structure of space group *Imma*, was found in the
100 Xianghualing skarn, Linwu County, Hunan Province, China. Its petrographic features,
101 chemical composition and crystal structure were determined by optical microscopy, electron
102 probe microanalysis, laser ablation inductively coupled plasma mass spectrometry
103

104 (LA-ICP-MS), and X-ray diffraction. The new mineral is named after “Chu kochen”
105 (1890-1974), a famous scientist and educationist in China, who is known as the inaugurator of
106 historical climatology, the leader of the “long march of academics”, the founder of the
107 Department of Geosciences at Zhejiang University, and, thus is recognized for making major
108 contributions to science and education in China. The species and the name have been
109 approved by the International Mineralogical Association, Commission on New Minerals,
110 Nomenclature and Classification (CNMNC) (IMA 2018-132a) (Rao et al. 2020). The type
111 sample of chukochenite is stored in the Geological Museum of China, No. 16, Yangrou
112 Hutong, Xisi, Beijing 100031, People’s Republic of China, catalogue number M13818. This
113 paper reports the chemical composition and crystal structure of chukochenite, and compares
114 its natural phase with the synthetic forms of $(\text{Li}_{0.5}\text{Al}_{0.5})\text{Al}_2\text{O}_4$.

115

116

OCCURRENCE AND ORIGIN

117 Chukochenite was found in the green rock of the Xianghualing skarn, which is a
118 tin-polymetallic (Sn-W-Be-Li) deposit in the Nanling Range, southern China. The
119 Xianghualing skarn is located at the exocontact zone of the Laiziling granite, which intruded
120 into the Middle-Upper Devonian carbonate rocks of the Qiziqiao Formation. The geological,
121 mineralogical, and geochronological features of the Xianghualing skarn and the Laiziling
122 granite have been extensively described in the literature (Chao 1964; Zhang et al. 1986;
123 Huang et al. 1988; Xiong et al. 2002; Yuan et al. 2007; Zhu et al. 2011; Yang et al. 2012, 2013;
124 Huang et al. 2015; Rao et al. 2017; Xie et al. 2018; Wu et al. 2018). Like ribbon (Jahns 1944)
125 or wriggilite rock (Kwak and Askins 1981), the Xianghualing skarn is composed of alternating
126 light layers of fluorite \pm other F-rich minerals and dark layers of Fe-rich minerals or Be-rich
127 minerals. Large amounts of rare-metal minerals, such as Sn minerals (cassiterite, hulsite, and
128 nigerite group minerals), W minerals (wolframite and scheelite), Be minerals (hsianghualite,

129 liberite, chrysoberyl, hambergite, bertrandite, and taaffeite group minerals), and Li minerals
130 (hsianghualite and liberite), occur in different layers, suggesting complex Sn, W, Be, and Li
131 mineralizations of the Xianghualing skarn.

132 Chukochenite occurs as subhedral to euhedral crystals in the green rock of the
133 Xianghualing skarn (Fig. 1). It is closely associated with fluorite, phlogopite, chrysoberyl,
134 margarite, chlorite, ferronigerite-2 $N1S$, and zinconigerite-2 $N1S$, indicating that chukochenite
135 is of hydrothermal origin and crystallized under F-rich conditions during the late stages of
136 mineralization in the Xianghualing skarn. On the basis of fluid inclusions studies, Liu and
137 Zeng (1998) suggested that the Li mineralization at late stage of the Xianghualing skarn likely
138 happened at 270-290°C and 30-60 MPa. These values may represent the physical condition of
139 chukochenite crystallization. Because of its relatively high concentrations of Li, Be, Sn, W,
140 Rb, Nb, and Ta, the Laiziling granite is regarded as the main Li source of the Xianghualing
141 orebodies, e.g., the average Li concentration in the Laiziling granite is 1615 ppm (Zhong
142 2014).

143

144 PHYSICAL AND OPTICAL PROPERTIES

145 Chukochenite crystals are up to 200 μm across (usually 50 to 100 μm), and are slightly
146 heterogeneous under backscattered electron images (Fig. 1), due to variation in their ZnO
147 contents. The crystals are colorless and transparent with vitreous luster, and show light red
148 and light green fluorescence under UV radiation of 253.7 nm and 365 nm, respectively. The
149 Mohs hardness is about 8, close to that of chrysoberyl; the tenacity is brittle with irregular
150 fracture. Based on the empirical formula and unit-cell parameters of chukochenite, its
151 calculated density is 3.771 g/cm^3 . Optically, chukochenite is biaxial (-), with $\alpha = 1.79(2)$, $\beta =$
152 $1.82(2)$, and $\gamma = 1.83(2)$ (589 nm). The calculated $2V$ is 60°, and optical orientation is $\alpha // a$, $\beta //$
153 b and $\gamma // c$. According to the calculated density and the measured indexes of refraction, the

154 compatibility index $[1 - (K_P/K_C)]$ is 0.011, which belongs to the “excellent” category
155 ([Mandarino 1981](#)).

156 **Raman spectroscopy**

157 A Raman spectrum of chukochenite was collected using a LabRAM HR evolution Laser
158 Raman microprobe in the School of Earth Sciences, Zhejiang University. The spectrum was
159 recorded from 100 to 4000 cm^{-1} with an accumulation time of 60 s using a 532 nm laser with a
160 power of 50 mW. The spectrum ([Fig. 2](#)) was obtained from a chukochenite single crystal on a
161 polished thin section chip. The Raman shifts at 827 and 754 cm^{-1} may be assigned to AlO_4
162 tetrahedra, while the Li-O and Al-O vibration modes in octahedra are probably at 692, 556
163 and 437 cm^{-1} . No Raman shifts are observed at 3400-3600 cm^{-1} , and thus there is no evidence
164 for the presence of either H_2O or OH in the structure of chukochenite.

165 **Chemical analysis**

166 Chemical compositions of chukochenite were determined at the EPMA Lab (SHIMADZU
167 EPMA-1720H; WDS; 15 kV; 20 nA; beam diameter = 1 μm) at Zhejiang University.
168 Standards for the analysis were orthoclase (Na K_α), MnTiO_3 (Ti K_α), almandine (Ca K_α and Fe
169 K_α), obsidian (K K_α), pyrope (Mg K_α), willemite (Mn K_α , Zn K_α and Si K_α), topaz (Al K_α), and
170 chromite (Cr K_α). The low analytical total from EPMA is due to the presence of Li_2O .
171 Fluorine was not detected in the sample.

172 Li contents of chukochenite were measured by LA-ICP-MS at Zhejiang University. The
173 laser was set at 6 Hz and 5 J/cm^2 energy per pulse, and the ablation times were typically 40 s.
174 The signal intensities (counts per ppm) for each element were calibrated against a NIST SRM
175 610 silicate glass standard (485 ppm Li), and the Fe content of chukochenite obtained by
176 EPMA was used as an internal standard. The NITS SRM 612 with 42 ppm Li was also
177 measured as an unknown to ensure the reliability of this method. The results from 6 spot
178 analyses are 1.64-1.77 wt.% Li, which is equivalent to 3.51-3.79 wt.% Li_2O . Beryllium was

179 not detected in chukochenite by LA-ICP-MS.

180 The chemical compositions of chukochenite are given in [Table 1](#), which lead to an
181 empirical formula
182 $[(\text{Li}_{0.355}\text{Al}_{0.138}\text{Na}_{0.005}\text{Ca}_{0.002})_{\Sigma 0.5}(\text{Al}_{0.145}\text{Fe}^{+3}_{0.147}\text{Mg}_{0.061}\text{Zn}_{0.058}\text{Mn}_{0.051}\text{Si}_{0.001})_{\Sigma 0.463}]\text{Al}_2\text{O}_4$, based
183 on 4 O atoms per formula unit ([Bosi *et al.* 2019b](#)). The idealized formula is $(\text{Li}_{0.5}\text{Al}_{0.5})\text{Al}_2\text{O}_4$,
184 which corresponds to Al_2O_3 94.46 wt.% and Li_2O 5.54 wt.%.

185 Powder X-ray diffraction

186 Powder X-ray diffraction (XRD) was performed with a Rigaku D/MAX RAPID II
187 micro-diffractometer (Mo $K\alpha$, $\lambda = 0.71073 \text{ \AA}$) at the State Key Laboratory for Mineral
188 Deposits Research, School of Earth Sciences and Engineering, Nanjing University, China.
189 The micro-diffractometer was operated with a curved imaging plate detector, under 40 kV and
190 100 mA at a scanning step of 0.03° , using a 0.3 mm diameter collimator in 2-Theta ranges of
191 $8\text{-}179.0^\circ$, and total exposure time was 2 h. We used the structural model obtained from
192 single-crystal XRD (see below) to index the powder XRD pattern of chukochenite ([Table 2](#)).
193 The nine strongest lines [d in \AA (I) (hkl)] are: 2.405 (53) (231); 1.996 (29) (260); 1.535 (77)
194 (303); 1.413 (100) (264); 1.260 (52) (2 12 0); 1.068 (36) (1 13 4); 1.039 (61) (503); 0.999 (59)
195 (008); and 0.942 (35) (3 13 4). Unit-cell parameters calculated from powder XRD data are: a
196 $= 5.642(1) \text{ \AA}$, $b = 16.827(2) \text{ \AA}$, $c = 8.014(1) \text{ \AA}$, and $V = 760.80(2) \text{ \AA}^3$.

197

198

199 CRYSTAL STRUCTURE DETERMINATION

200 Single-crystal XRD measurements were carried out using a Rigaku Synergy
201 diffractometer (Mo $K\alpha$ 50 kV, 1 mA) in the School of Earth Sciences and Info-physics, Central
202 South University, China. One crystal fragment, measuring $40 \times 35 \times 20 \text{ \mu m}$, provided usable

203 data to perform a structure refinement of chukochenite (CIF¹ available on deposit). 550
204 frames with a spatial resolution of 0.5° were collected by the ϕ/ω scan technique, with a
205 counting time of 20 s per frame, in the range $4.82^\circ < 2\theta < 67.42^\circ$. A total of 3670 reflections
206 were extracted from these frames, corresponding to 758 unique reflections. The Rigaku
207 CrystalClear software package was used for processing the structural data of chukochenite,
208 including Lorentz and polarization corrections, and the application of an empirical absorption
209 correction using the multi-scan method with ABSCOR (Higashi 2001). Unit cell parameters
210 refined from these reflections are $a = 5.659(1) \text{ \AA}$, $b = 16.898(1) \text{ \AA}$, $c = 7.994(1) \text{ \AA}$, $V =$
211 $764.46(8) \text{ \AA}^3$, and $Z = 12$. Careful inspection of the reflection dataset indicated *Imma* as the
212 most probable space group.

213 The crystal structure was determined and refined to $R = 0.0424$, based on 613
214 independent reflections with $I > 3\sigma(I)$ using the program package JANA2006 (Petříček *et al.*
215 2014). Atomic scattering factors for neutral atoms together with anomalous dispersion
216 correction were taken from *International Tables for Crystallography* (Prince 2004). The site
217 scattering factors were obtained by refining Al vs Li on the Li1, Al1, Al3 and Al5 sites, and by
218 refining Fe vs Al on the Al2 and Al3 sites. The cationic distribution was established in
219 agreement with the chemical data, site scattering factors and average bond distances (Table 3).
220 Selected bond distances are given in Table 4, and bond valence analysis results are presented in
221 Table 5.

222 The structure of chukochenite is based on a tetrahedral-octahedral framework (Fig. 3).
223 Tetrahedra are mainly occupied by Al, with two sizes of AlO₄ tetrahedra ($\langle \text{Al2-O} \rangle =$
224 $1.793\text{-}1.828 \text{ \AA}$ and $\langle \text{Al4-O} \rangle = 1.917\text{-}1.936 \text{ \AA}$), which are occupied by 0.87 Al + 0.13 Fe³⁺
225 and 0.32 Al + 0.18 Mg + 0.17 Fe³⁺ + 0.17 Zn + 0.16 Mn, respectively (Table 3). Octahedra are
226 occupied by Al and Li, corresponding to AlO₆ octahedra ($\langle \text{Al-O} \rangle = 1.883\text{-}1.955 \text{ \AA}$) and LiO₆

¹ Deposit item AM-?, CIF

227 octahedra ($\langle \text{Li-O} \rangle = 2.004\text{-}2.040 \text{ \AA}$). The octahedral Al1, Al3 and Al6 sites are occupied by
228 $0.95\text{Al} + 0.05 \text{Li}$, $0.92 \text{Al} + 0.08 \text{Li}$ and $0.90 \text{Al} + 0.10 \text{Li}$, respectively. The octahedral LiO_6
229 site is occupied by $0.70 \text{Li} + 0.30 \text{Al}$. In the *b* direction, AlO_6 and LiO_6 octahedra in 2:1 ratio
230 share edges, forming octahedral chains. In layers parallel to (010), AlO_6 octahedra form
231 chains along the *a* axis via edge-sharing. AlO_4 tetrahedra occur between AlO_6 - LiO_6 and AlO_6
232 octahedral chains; each corner of an AlO_4 tetrahedron shares with three AlO_6 octahedra or
233 two $\text{AlO}_6 +$ one LiO_6 octahedra. In fact, chukochenite is the first spinel mineral with the space
234 group *Imma*, and belongs to a new lithium oxyspinel mineral (Bosi *et al.* 2019a).
235 Chukochenite is isostructural with spinel supergroup minerals, but Li-bearing spinel has not
236 been reported previously.

237

238 DISCUSSION

239 Chukochenite is a new mineral having the composition $(\text{Li}_{0.5}\text{Al}_{0.5})\text{Al}_2\text{O}_4$, identical to that
240 of spinel compounds that have been much studied because of their fluorescence,
241 phosphorescence and magnetic properties when doped with trace elements. Synthetic
242 $(\text{Li}_{0.5}\text{Al}_{0.5})\text{Al}_2\text{O}_4$ has two polymorphs: a low temperature ordered phase with the space group
243 $P4_132$ (e.g., Darul *et al.* 2007) and a high temperature disordered phase with the space group
244 $Fd\bar{3}m$ (e.g., Kutty and Nayak 1998). In contrast, chukochenite has the space group *Imma*,
245 which has not been reported in synthetic $(\text{Li}_{0.5}\text{Al}_{0.5})\text{Al}_2\text{O}_4$. Powder XRD patterns of
246 chukochenite and synthetic $(\text{Li}_{0.5}\text{Al}_{0.5})\text{Al}_2\text{O}_4$ compounds are largely similar (Table 2).
247 However, there are several peaks with the *d* values of 8.501, 7.081, 4.593, 3.107 and 2.815 Å
248 in low diffraction angle region of chukochenite (Table 2) that cannot be explained by the
249 structures of synthetic $(\text{Li}_{0.5}\text{Al}_{0.5})\text{Al}_2\text{O}_4$ compounds (e.g., Kutty and Nayak 1998; Xie *et al.*
250 2011). Therefore, chukochenite is not only the first natural spinel supergroup mineral
251 containing Li, but also the first to have the *Imma* symmetry. Nonetheless, the structures of

252 chukochenite and synthetic $(\text{Li}_{0.5}\text{Al}_{0.5})\text{Al}_2\text{O}_4$ show a framework of tetrahedra and octahedra
253 that is isostructural with that of the spinel supergroup (Peterson et al., 1991; Bosi et al. 2019a).
254 Of greatest interest are the sites occupied by Li. In the chukochenite structure (Fig. 3), Li
255 occupies octahedrally coordinated sites, and LiO_6 and AlO_6 octahedra form edge-sharing
256 octahedral chains. The Li site is occupied by 0.70 Li, while the three Al octahedrally
257 coordinated sites are occupied by 0.05 Li, 0.08 Li and 0.10 Li, respectively. Each LiO_6
258 octahedron shares edges with six AlO_6 octahedra, and shares corners with six AlO_6 tetrahedra.
259 Li is absent in the tetrahedrally coordinated sites in the synthetic $(\text{Li}_{0.5}\text{Al}_{0.5})\text{Al}_2\text{O}_4$ structures,
260 and the octahedrally coordinated sites are occupied by Li and Al with 1:3 ratio (Famery et al.
261 1979). The different Li atomic arrangements between two synthetic $(\text{Li}_{0.5}\text{Al}_{0.5})\text{Al}_2\text{O}_4$ phases
262 result in the ordered and disordered in the octahedral sites (Darul et al. 2007; Xie et al. 2011).
263 The primitive cubic ordered $(\text{Li}_{0.5}\text{Al}_{0.5})\text{Al}_2\text{O}_4$ phase has a 1:3 ordering of Li:Al in the
264 octahedrally coordinated sites; each Li is surrounded by six Al atoms and each Al is
265 surrounded by two Li and four Al atoms. In contrast, the spinel form of $(\text{Li}_{0.5}\text{Al}_{0.5})\text{Al}_2\text{O}_4$ has a
266 disordered structure of Li and Al over octahedrally coordinated sites. Therefore, the different
267 $(\text{Li}_{0.5}\text{Al}_{0.5})\text{Al}_2\text{O}_4$ structures are determined by the occupancy and distribution of Li in
268 octahedrally coordinated sites.

269 In fact, chukochenite is generally isostructural with the two synthetic $(\text{Li}_{0.5}\text{Al}_{0.5})\text{Al}_2\text{O}_4$
270 phases. Its lower symmetry (orthorhombic *Imma*) is in large part due to Li^+ ordering, but the
271 framework structure of spinel remains. The unit cell of chukochenite can be derived from that
272 of synthetic spinel $(\text{Li}_{0.5}\text{Al}_{0.5})\text{Al}_2\text{O}_4$. Relative to the unit cell of synthetic $(\text{Li}_{0.5}\text{Al}_{0.5})\text{Al}_2\text{O}_4$, the
273 unit cell of chukochenite is rotated 45° around *c* axis (Fig. 4). Therefore, the unit cell of
274 chukochenite can be obtained by $a = c (7.994 \text{ \AA}) \times \cos 45^\circ = 5.683 \text{ \AA}$, $b = 3 \times a = 16.958 \text{ \AA}$,
275 and $V = 1.5 \times V^* (7.994^3 \text{ \AA}^3) = 766.27 \text{ \AA}^3$.

276

277

IMPLICATIONS

278 $(\text{Li}_{0.5}\text{Al}_{0.5})\text{Al}_2\text{O}_4$ adopts a series of polymorphs: disordered spinel $(\text{Li}_{0.5}\text{Al}_{0.5})\text{Al}_2\text{O}_4$
279 $(Fd\bar{3}m) \rightarrow$ ordered $(\text{Li}_{0.5}\text{Al}_{0.5})\text{Al}_2\text{O}_4$ $(P4_132) \rightarrow$ chukochenite (*Imma*). With increasing Li
280 ordering, the symmetry decreases, but there is no change in the spinel framework topology.
281 Therefore, the discovery of chukochenite draws attention to cation ordering during transitions
282 between different $(\text{Li}_{0.5}\text{Al}_{0.5})\text{Al}_2\text{O}_4$ polymorphs. While synthetic $(\text{Li}_{0.5}\text{Al}_{0.5})\text{Al}_2\text{O}_4$ transforms
283 from the disordered $Fd\bar{3}m$ phase to the ordered $P4_132$ phase, the ordering of $(\text{Li}_{0.5}\text{Al}_{0.5})\text{Al}_2\text{O}_4$
284 phases in nature likely follows a different ordering path, ending with chukochenite. Under
285 ambient pressure and dry environment, the transition between two synthetic $(\text{Li}_{0.5}\text{Al}_{0.5})\text{Al}_2\text{O}_4$
286 phases was indicated to happen around $1295 \pm 5^\circ\text{C}$ (e.g., [Braun 1952](#); [Datta and Roy 1963](#);
287 [Kutty and Nayak 1998](#)), but chukochenite (highly ordered, *Imma*) from the Xianghualing
288 skarn likely crystallized from aqueous fluids at $270\text{-}290^\circ\text{C}$ and $30\text{-}60$ MPa ([Liu and Zeng](#)
289 [1998](#)). The intimate intergrowths of chukochenite with fluorite ([Fig. 1](#)) suggest that the
290 crystallization occurred under F-rich conditions during the late stages of hydrothermal
291 metasomatism in the Xianghualing skarn. This feature may indicate that high fluorine activity
292 could promote Li^+ ordering in the spinel structure. However, more than one path may happen
293 between the completely disordered and the fully ordered $(\text{Li}_{0.5}\text{Al}_{0.5})\text{Al}_2\text{O}_4$ phases during
294 different geological processes. Hence, future work on multiple ordering paths
295 in $(\text{Li}_{0.5}\text{Al}_{0.5})\text{Al}_2\text{O}_4$ is needed.

296

297

298

ACKNOWLEDGEMENTS

299 We thank Ulf Hålenius, Edward S. Grew, Ferdinando Bosi, an anonymous reviewer, and
300 Editor Hongwu Xu for their very helpful comments on the manuscript, which greatly

301 improved its quality. Financial support for the research was provided by NSF of China (Grant
302 No. 41772031).

303

304

305

REFERENCES CITED

306 Bosi, F., Biagioni, C., and Pasero, M. (2019a) Nomenclature and classification of the spinel supergroup.
307 European Journal of Mineralogy, 31, 183–192.

308 Bosi, F., Biagioni, C., and Oberti, R. (2019b) On the chemical identification and classification of minerals.
309 Minerals, 9, 591.

310 Braun, P.B. (1952) A superstructure in spinels. Nature, 170, 1123–1131.

311 Brown, I.D., and Altermatt, D. (1985) Bond-valence parameters obtained from a systematic analysis of the
312 inorganic crystal-structure database. Acta Crystallographica, B41, 244–247.

313 Chao, C.L. (1964) Liberite $\text{Li}_2\text{BeSiO}_4$, a new lithium-beryllium silicate mineral from the Nanling Ranges,
314 South China. Acta Mineralogica Sinica, 44(3), 334–342 (in Chinese with English abstract). American
315 Mineralogist, 50, 519 (abstract).

316 Darul, J., Nowicki, W., Piszora, P., and Wolska, E. (2007) Synchrotron X-ray powder diffraction studies of
317 solubility limits in the LiFe_5O_8 - LiAl_5O_8 spinel solid solutions. Zeitschrift für Kristallographie, S26,
318 471–476.

319 Datta, R.K., and Roy, R. (1963) Phase transitions in LiAl_5O_8 . Journal of the American Ceramic
320 Society, 46(8), 388–390.

321 Famery, R., Queyroux, F., Gilles, J.C., and Herpin, P. (1979) Etude structurale de la forme ordonnée de
322 LiAl_5O_8 , Journal of Solid State Chemistry, 30(2), 257–263.

323 Higashi, T. (2001) ABSCOR. Rigaku Corporation, Tokyo.

324 Huang, Y.H., Du, S.H., and Zhou, X.Z. (1988) Hsianghualing rocks, deposits and minerals. Beijing
325 Scientific Technique Press. 115–116 (in Chinese).

326 Huang, F.F., Wang, R.C., Xie, L., Zhu, J.C., Erdmann, S., Che, X.D., and Zhang, R.Q. (2015)
327 Differentiated rare-element mineralization in an ongonite–topazite composite dike at the Xianghualing
328 tin district, Southern China: an electron-microprobe study on the evolution from
329 niobium-tantalum-oxides to cassiterite. Ore Geology Reviews, 65(3), 761–778.

330 Jahns, R.H. (1944) “Ribbon rock”, an unusual beryllium-bearing tactite. Economic Geology, 39(3),
331 173–205.

332 Kutty, T.R.N., and Nayak, M. (1998) Cationic distribution and its influence on the luminescent properties
333 of Fe^{3+} -doped LiAl_5O_8 prepared by wet chemical methods. Journal of Alloys and Compounds, 269,
334 75–87.

- 335 Kwak, T.A.P., and Askins, P.W. (1981) The nomenclature of carbonate replacement deposits, with
336 emphasis on Sn-F-Be-Zn “wrigglite” skarns. *Journal of the Geological Society of Australia*, 28(1-2),
337 123–136.
- 338 Liu, J.Q., and Zeng, Y.S. (1998) Preliminary study on fluid inclusions in hsianghualite. *Huanan Dizhi Yu*
339 *Kuangchan*, 56–63.
- 340 Mandarino, J.A. (1981) The Gladstone-Dale relationship. IV. The compatibility concept and its application.
341 *Canadian Mineralogist*, 19, 441–450.
- 342 Peterson, R.C., Lager, G.A., and Hitterman, R.L. (1991) A time-of-flight neutron powder diffraction study
343 of MgAl_2O_4 at temperatures up to 1273 K. *American Mineralogist*, 76, 1455–1458.
- 344 Petříček, V., Dusek, M., and Palatinus, L. (2014). Crystallographic computing system, JANA 2006:
345 General features. *Zeitschrift für Kristallographie*, 229(5), 345–352.
- 346 Pott, G.T., and Mcnicol, B.D. (1973) Luminescence of Cr^{3+} ions in ordered and disordered LiAl_5O_8 .
347 *Journal of Luminescence*, 7(2), 132–137.
- 348 Prince, E. (Ed.) (2004) *International Tables for Crystallography, Volume C: Mathematical, Physical and*
349 *354 Chemical Tables, 3rd Edition*. Kluwer Academic Publishers, Dordrecht.
- 350 Rao, C., Gu, X.P., Wang, R.C., Xia, Q.K., Cai, Y.F., Dong, C.W., Hatert, F., and Hao, Y.T. (2020)
351 Chukochenite, IMA 2018-132a. *CNMNC Newsletter No. 54*; *European Journal of Mineralogy*, **32**, (*in*
352 *press*).
- 353 Rao, C., Hatert F., Dal Bo, F., Wang, R.C., Gu, X.P., and Baijot, M. (2017) Mengxianminite
354 ($\text{Ca}_2\text{Sn}_2\text{Mg}_3\text{Al}_8[(\text{BO}_3)(\text{BeO}_4)\text{O}_6]_2$) a new borate mineral from Xianghualing skarn, Hunan Province,
355 China, with a highly unusual chemical combination (B + Be + Sn). *American Mineralogist*, 102,
356 2136–2141.
- 357 Shannon, R.D. (1976) Revised crystal ionic radii and systematic study of interatomic distances in halides
358 and chalcogenides. *Acta Crystallographica*, A32, 751–767.
- 359 Singh, V., and Rao, T.K.G. (2008) Studies of defects in combustion synthesized europium-doped LiAl_5O_8
360 red phosphor. *Journal of Solid State Chemistry*, 181(6), 1387–1392.
- 361 Wu, J.H., Li, H., Algeo, T.J., Jiang, W.C., and Zhou, Z.K. (2018) Genesis of the Xianghualing Sn-Pb-Zn
362 deposit, South China: A multi-method zircon study, *Ore Geology Reviews*, 102, 220–239.
- 363 Xie, L., Wang, Z.J., Wang, R.C., Zhu, J.C., Che, X.D., Gao, J.F., and Zhao, X. (2018) Mineralogical
364 constraints on the genesis of W–Nb–Ta mineralization in the Laiziling granite (Xianghualing district,
365 south China). *Ore Geology Reviews*, 95, 695–712.
- 366 Xie, L.M., Yang, D.M., Wei, L., Hu, Y.M., and Ji, H.X. (2011) Synthesis and luminescence properties of
367 plate-like europium ion doped LiAl_5O_8 . *Journal of Synthetic Crystals*, 40(3), 684–688.
- 368 Xiong, X.L., Rao, B., Chen, F.R., Zhu, J.C., and Zhao, Z.H. (2002) Crystallization and melting experiments
369 of a fluorine-rich leucogranite from the Xianghualing pluton, South China, at 150 MPa and
370 H_2O -saturated conditions. *Journal of Asian Earth Sciences*, 21(2), 175–188.

- 371 Yang, Z.M, Ding, K., Fourestier, J.D., Mao, Q., and Li, H., (2012) Fe-rich Li-bearing magnesio
372 nigerite-6N6S from Xianghualing tin-polymetallic ore field, Hunan Province, P.R. China. *Mineralogy
373 and Petrology*, 107(2), 163–169.
- 374 Yang, Z.M., Fourestier, J.D., Ding, K., and Li, H. (2013) Li-bearing ferronigerite-2N1S from Xianghualing
375 tin-polymetallic ore field, Hunan Province, China. *Canadian Mineralogist*, 51(6), 913–919.
- 376 Yuan, S., Peng, J., Shen, N., Hu, R., and Dai, T. (2007) ^{40}Ar - ^{39}Ar isotopic dating of the Xianghualing
377 Sn-polymetallic ore field in Southern Hunan, China and its geological implications. *Acta Geologica
378 Sinica*, 81(2), 278–286 (in Chinese, English Abstract).
- 379 Zhang, D.Q., and Wang, L.H. (1986) Metasomatism and zonation of the Xianghualing Tin-polymetallic
380 deposit. *Bulletin of the Institute of Mineral Deposits Chinese Academy of Geological Sciences*, 2,
381 144–154.
- 382 Zhong, J.L. (2014) Major types and prospecting direction of nonferrous and rare polymetallic ore deposit in
383 Xianghualing area, South China. *Geology and mineral resource of south China*, 30(2), 99–108.
- 384 Zhu, J.C., Wang, R.C., Lu, J.J., Zhang, H., Zhang, W.L., Xie, L., and Zhang, R.Q. (2011) Fractionation,
385 evolution, petrogenesis and mineralization of Laiziling granite pluton, Southern Hunan Province.
386 *Geological Journal of China Universities*, 17(3), 381–392.

387
388

389 **Figure captions:**

- 390 **FIGURE 1.** Backscattered electron images showing (a) occurrence and mineral associations of
391 chukochenite and (b) euhedral chukochenite crystals among fluorite crystals. Abbr.: Ckc -
392 chukochenite; Fl - fluorite; Na-M - Na-matgarite.
- 393 **FIGURE 2.** Raman spectrum of chukochenite.
- 394 **FIGURE 3.** Structural model of chukochenite.
- 395 **FIGURE 4.** Geometrical relationship of the two unit-cells between (a) synthetic $(\text{Li}_{0.5}\text{Al}_{0.5})\text{Al}_2\text{O}_4$ and
396 (b) chukochenite.

397

398 **Table captions:**

- 399 **TABLE 1.** Chemical composition of chukochenite from the Xianghualing skarn
- 400 **TABLE 2.** X-ray powder diffraction pattern (d in Å) of chukochenite and synthetic
401 $(\text{Li}_{0.5}\text{Al}_{0.5})\text{Al}_2\text{O}_4$
- 402 **TABLE 3.** Cationic distribution in the crystal structure of chukochenite
- 403 **TABLE 4.** Selected bond distances (Å) in chukochenite
- 404 **TABLE 5.** Bond valence sums for chukochenite

405
406

TABLE 1. Chemical composition of chukochenite from the Xianghualing skarn

	Wt.% (n=31)	Range	Stand. Dev.		<i>a.p.f.u.</i>
Al ₂ O ₃	80.70	75.68-86.03	2.47	Al	4.565
Fe ₂ O ₃ [*]	8.16	6.90-11.03	0.84	Fe ⁺³	0.295
Li ₂ O [#]	3.68	3.51-3.79	0.12	Li	0.711
ZnO	3.25	0.20-8.24	2.41	Zn	0.116
MnO	2.49	1.70-4.57	0.65	Mn	0.102
MgO	1.70	0.77-2.89	0.50	Mg	0.121
Na ₂ O	0.11	0-0.30	0.07	Na	0.010
CaO	0.08	0-0.52	0.13	Ca	0.004
SiO ₂	0.04	0-0.15	0.03	Si	0.002
TiO ₂	0.02	0-0.06	0.02	Ti	0.001
K ₂ O	0.01	0-0.01	0.01	K	0.000
Cr ₂ O ₃	0.01	0-0.04	0.01	Cr	0.000
Total	100.24	99.06-100.97	0.46		

Fe₂O₃^{*}: calculated as trivalent; Li₂O[#]: measured by LA-ICP-MS.

TABLE 2. X-ray powder diffraction pattern (d in Å) of chukochenite and synthetic $(\text{Li}_{0.5}\text{Al}_{0.5})\text{Al}_2\text{O}_4$

Chukochenite				Synthetic $\text{LiAl}_5\text{O}_8^*$			Synthetic $\text{LiAl}_5\text{O}_8^{**}$		
$I_{\text{obs.}}$	$d_{\text{obs.}}$	$d_{\text{cal.}}$	hkl	I	d	hkl	I	d	hkl
12.7	8.501	8.450	020						
6.4	7.081	7.209	011	16.5	5.591	110			
7.6	4.593	4.601	031	5.8	4.565	111	35.0	4.610	111
5.3	3.107	3.112	051	15.2	3.536	210			
17.3	2.815	2.821	200	38.6	2.795	220	25.0	2.821	220
53.1	2.405	2.404	231	100	2.384	311	100.0	2.405	311
28.9	1.996	1.989	260	46.6	1.977	400	65.0	1.995	400
25.4	1.627	1.629	332	12.1	1.614	422	10	1.629	422
76.7	1.535	1.538	303	33.1	1.521	511	40	1.536	511
100.0	1.413	1.412	264	63.2	1.398	440	75.0	1.410	440
2.7	1.349	1.350	165				3	1.349	531
51.8	1.260	1.256	2 12 0				2	1.262	620
25.4	1.219	1.220	305				10.0	1.217	533
11.0	1.151	1.153	404				7.0	1.152	444
100.0 [#]	1.116	1.116	0 15 1						
36.2	1.068	1.068	1 13 4						
60.7	1.039	1.040	503						
59.1	0.999	0.999	008						
100.0 [#]	0.967	0.965	4 12 2						
34.8	0.942	0.941	3 13 4						

[#]: Peaks overlapping with fluorite peaks. ^{*}: synthetic $(\text{Li}_{0.5}\text{Al}_{0.5})\text{Al}_2\text{O}_4$ with the space group $P4_132$ (data from PDF No. 71-1736); ^{**}: synthetic $(\text{Li}_{0.5}\text{Al}_{0.5})\text{Al}_2\text{O}_4$ with the space group $Fd\bar{3}m$ (data from PDF No. 31-0701).

TABLE 3. Cationic distribution in the crystal structure of chukochenite

Site	RSS	Site-population (<i>apfu</i>)	CSS	ABL	CBL	VS	BVS
Li ^{VI}	6.4	Li _{0.70} Al _{0.30}	6.0	2.016	2.093	1.60	1.58
Al1 ^{VI}	12.7	Al _{0.95} Li _{0.05}	12.5	1.920	1.946	2.90	2.83
Al2 ^{IV}	14.7	Al _{0.87} Fe ³⁺ _{0.13}	14.7	1.808	1.783	3.00	2.72
Al3 ^{VI}	12.2	Al _{0.92} Li _{0.08}	12.2	1.924	1.953	2.84	2.77
Al4 ^{IV}	20.3	Al _{0.32} Mg _{0.18} Fe ³⁺ _{0.17} Zn _{0.17} Mn _{0.16}	19.8	1.928	1.898	2.49	2.21
Al5 ^{VI}	12.5	Al _{0.90} Li _{0.10}	12.0	1.909	1.958	2.80	2.85

RSS: Refined site scattering factor (e^-); CSS: Calculated site scattering factor (e^-); ABL: average observed bond-lengths (Å); CBL: calculated bond-lengths (Å); VS: theoretical bond-valence sums (νu); BVS: calculated bond-valence sums (νu). Ideal bond-distances were calculated using the ionic radii of Shannon (1976), and the bond-valence parameters were taken from Brown and Altermatt (1985).

TABLE 4. Selected bond distances (Å) in chukochenite

Li-O1(×2)	2.040(3)	Al3-O2(×2)	1.883(3)	Al4-O2(×2)	1.936(3)
Li-O3(×4)	2.004(2)	Al3-O5(×4)	1.945(2)	Al4-O4(×2)	1.917(3)
<Li-O>	2.016	<Al-O>	1.924	<Al-O>	1.927
Al1-O1(×2)	1.905(2)	Al2-O1	1.793(3)	Al5-O2(×2)	1.920(2)
Al1-O3(×2)	1.931(2)	Al2-O3(×2)	1.805(2)	Al5-O3(×2)	1.880(2)
Al1-O4(×2)	1.925(2)	Al2-O5	1.828(3)	Al5-O4	1.900(3)
<Al-O>	1.920	<Al-O>	1.808	Al5-O5	1.955(3)
				<Al-O>	1.909

TABLE 5. Bond valence sums for chukochenite

	Li	Al1	Al2	Al3	Al4	Al5	Σ
O1	0.258($\times 2 \rightarrow$)($\times 2 \downarrow$)	0.529($\times 2 \rightarrow$)($\times 2 \downarrow$)	0.672				1.99
O2				0.542($\times 2 \downarrow$)	0.519($\times 2 \downarrow$)	0.44($\times 2 \rightarrow$)	1.94
O3	0.278($\times 4 \rightarrow$)($\times 4 \downarrow$)	0.494($\times 2 \downarrow$)	0.656($\times 2 \downarrow$)			0.487($\times 2 \downarrow$)	1.92
O4		0.498($\times 2 \rightarrow$)($\times 2 \downarrow$)			0.519($\times 2 \downarrow$)	0.468($\times 2 \downarrow$)	1.98
O5			0.62915	0.461($\times 2 \rightarrow$)($\times 4 \downarrow$)		0.408	1.96
Σ	1.63	3.04	2.61	2.93	2.08	2.73	

FIGURE 1

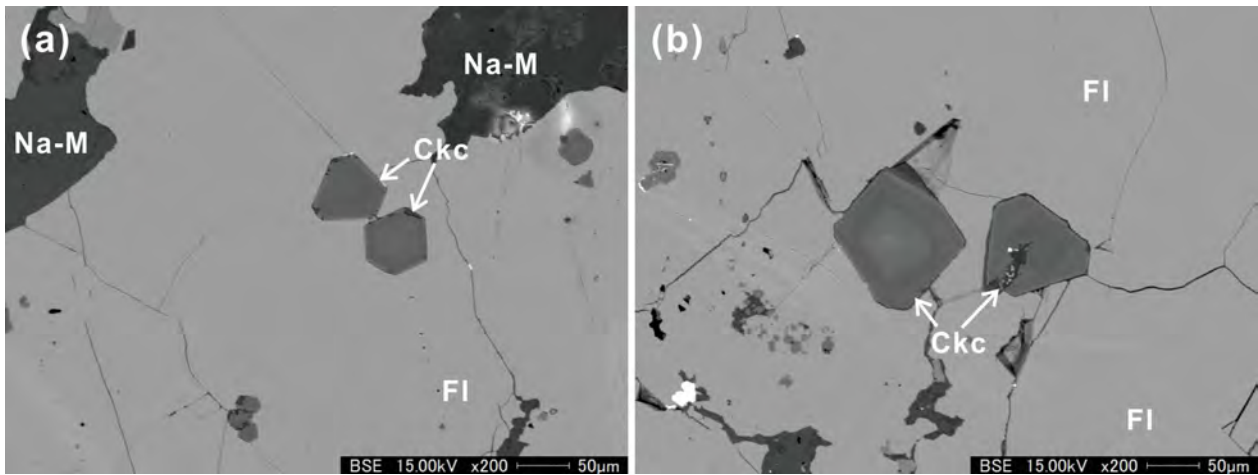


FIGURE 2

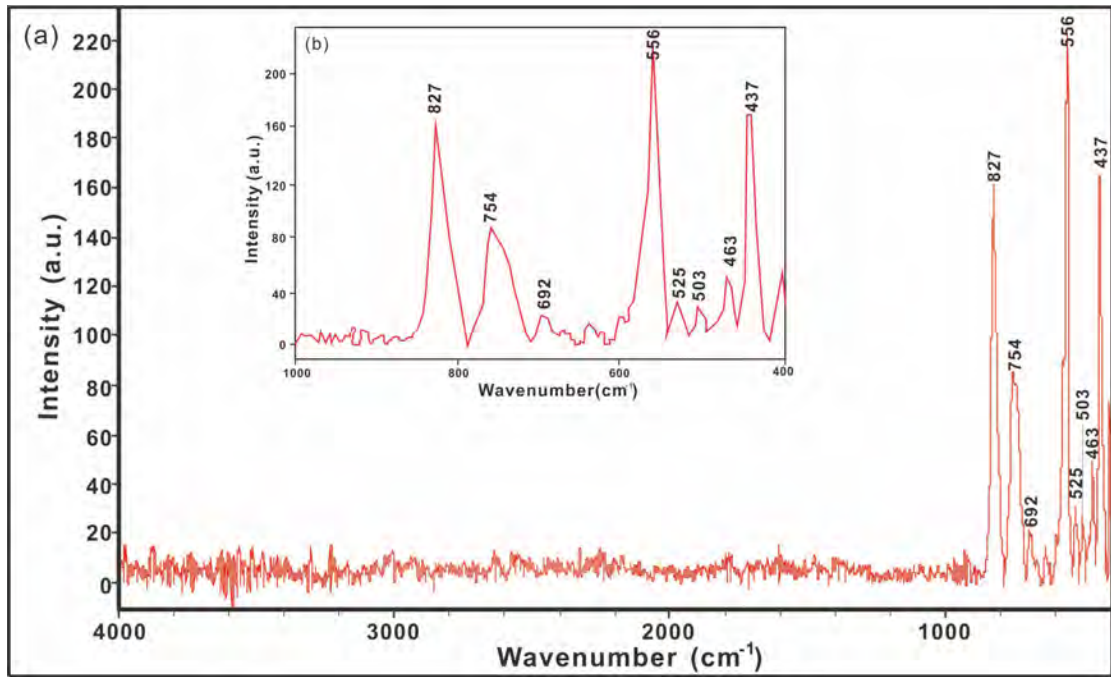


FIGURE 3

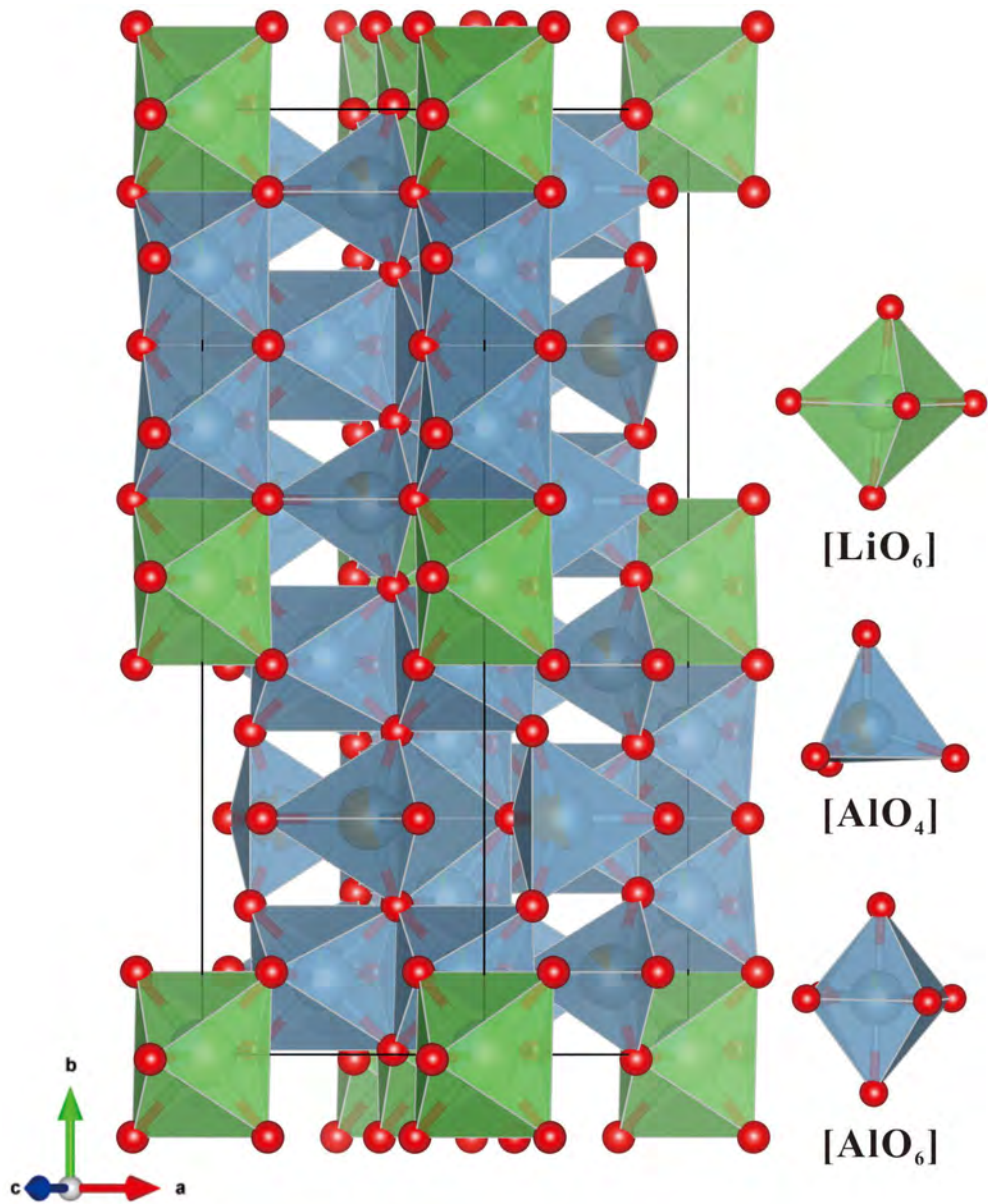


FIGURE 4

